SLAC–PUB–8494
June 2000

Simulation of Bunch Lengthening and Sawtooth Mode in the SLAC Damping Rings *

Robert Warnock and Karl Bane
Stanford Linear Accelerator Center, Stanford University, Stanford, CA 94309
E-mail: warnock@slac.stanford.edu; kbane@slac.stanford.edu

James Ellison
Department of Mathematics and Statistics
University of New Mexico, Albuquerque, NM, 87131
E-mail: ellison@math.unm.edu

Abstract

We study longitudinal coherent motion of a stored electron beam by a time domain integration of the nonlinear Vlasov-Fokker-Planck equation. For the present SLAC damping rings we found several features in agreement with experiment. This report emphasizes the earlier vacuum chamber of the rings, replaced in 1992-93. Nonlinear effects are much stronger for the old chamber, and the computed phenomena more various.

Presented at
7th European Particle Accelerator Conference
Vienna, Austria, 26-30 June, 2000

*Work supported in part by Department of Energy contracts DE–AC03–76SF00515 and DE–FG03–99ER41104.

1 INTRODUCTION

Comparable studies of longitudinal instabilties in storage rings have relied on one of two methods: (1) linearization of the Vlasov equation about the equilibrium solution of the full Vlasov-Fokker-Planck equation [1]; (2) simulation by tracking a large number of macroparticles, including a model of radiation with quantum fluctuations, e.g.[2]. Recently two of the authors developed a method for time-domain integration of the nonlinear Vlasov-Fokker-Planck (VFP) equation [3]. In principle, this accomplishes the same thing as method (2), but in practice there are two important advantages: the resulting phase space distributions have very low noise, and the integration can be done over a period equal to several realistic damping times.

Our method of integration, described in detail in Ref.[3], uses operator splitting to treat the Vlasov and Fokker-Planck terms independently. The Fokker-Planck operator is handled by an elementary method for partial differential operators. The key to success is to use a different technique for the Vlasov term, a method with a clear motivation in the basic structure of the Vlasov equation as an expression of probability conservation. We call the technique the *Method of Local Characteristics*. It is the classical method of characteristics, modified to include the collective force. The latter is treated as though it were a time-independent external force during a small time step.

2 DEFINITIONS AND EQUATIONS FOR LONGITUDINAL MOTION

We consider ultra-relativistic electrons and use normalized, dimensionless phase space variables as follows: $q = z/\sigma_z$, $p = -(E - E_0)/\sigma_E$. Here z is the distance from the synchronous particle (positive for leading particles), and E is the energy with mean value E_0. The quantities σ_z and σ_E are the rms bunch length and energy spread in the low-current equilibrium state.

The phase space distribution function with unit integral is denoted by $f(q, p, \theta)$, where the "time" is $\theta = \omega_s t$, with ω_s the circular synchrotron frequency. The charge density for N particles is $\rho(q, \theta) = eN \int f(q, p, \theta) dp$. The collective force due to the wake field, a functional of f at time θ, is taken to be $F(q, f(\theta)) = \int W(q - q')\rho(q', \theta) dq'$, where a positive value of the point source wake potential W corresponds to energy gain.

We use wake potentials for the old and new vacuum chambers that were computed by time-domain electromagnetic codes. The source for computed fields was a 1mm Gaussian bunch, not a point source and not extremely short compared to the nominal bunch length of about 5mm. Also, some difficult three dimensional structures were treated crudely. Probably the main shortcoming of the wake potentials is omission or smoothing of field components of short wave length. These components are most likely to influence bunches of high current, which are prone to develop small-scale structure.

We assume that the motion occurs in the linear region of the r.f. force. In that case the VFP equation is [3]

$$\frac{\partial f}{\partial \theta} + p\frac{\partial f}{\partial q} - \big(q + IF(q, f)\big)\frac{\partial f}{\partial p} = 2\beta \frac{\partial}{\partial p}\big(pf + \frac{\partial f}{\partial p}\big) \ , \quad (1)$$

where the intensity parameter is $I = Ne^2/(2\pi\nu_s\sigma_E)$ with synchrotron tune ν_s. In our normalized coordinates the damping and diffusion constants are both equal to $2\beta = 2/(\omega_s\tau_d)$, with τ_d the longitudinal damping time.

We integrate equation (1) by the method described in [3], with a 401×401 phase space grid and 1024 time steps per synchrotron period. After some improvements in the code we now integrate for 3 damping times in 24 hours, on 400MHz work stations. All integrations begin with the Haïssinski equilibrium state, which exists even at very high currents, even though it is unstable to small perturbations at such currents.

To verify the code we have used various criteria: invariance of the equilibrium at low current; reproduction of an exact time-dependent solution of the nonlinear Vlasov equation, constructed from the Haïssinski distribution [3]; reproduction of the analytic solution of the Fokker-Planck equation for zero wake field; charge conservation; smoothness of the distribution and smallness at the boundary of the grid. Also, we find solutions that are nearly periodic with very long period (as much as 3.9 damping times!) This indicates long-term stability of the algorithm.

3 PRESENT VACUUM CHAMBER

Simulations for the present vacuum chamber, with comparisons to experiment, were reported in [3]. For machine parameters as in Eq.(36) of [3], the computed equilibrium state is invariant to high accuracy under the time-domain integration algorithm, for bunch population N less than about $1.6 \cdot 10^{10}$. At $N = 1.64 \cdot 10^{10}$ bunch lengthening and increased energy spread set in. The corresponding experimental threshold is $(1.7 \pm .03) \cdot 10^{10}$. Runs at somewhat higher current, $(1.74, 1.84) \cdot 10^{10}$, show oscillations of σ_q or σ_p with a frequency somewhat smaller than $2\omega_s$, with asymptotically constant amplitude. The constant amplitude sets in after a long transient of slowly increasing amplitude, lasting 2-3 damping times. Beginning at about $2 \cdot 10^{10}$ there is a somewhat gradual transition to a sawtooth or bursting mode. This still has fast oscillations near $2\omega_s$, but with an envelope that varies periodically after 2-3 damping times. Such a mode at $N = 2.99 \cdot 10^{10}$ is shown in Figure 1.

In experiments the constant-amplitude mode is seen up to $N = 2.6 \cdot 10^{10}$, at which point there is a relatively sharp transition to the sawtooth mode. For the case of Figure 1 the period of the sawtooth envelope oscillations is $0.607\tau_d$, as compared to $0.62\tau_d$ by experiment. The fast oscillations have frequency $1.816\omega_s$ in the simulation and $(1.84 \pm .02)\omega_s$ by experiment.

At about $3.2 \cdot 10^{10}$ the sawtooth mode disappears in the experiments, and a new frequency of fast oscillations appears at $2.54\omega_s$. No such thing is observed in the simula-

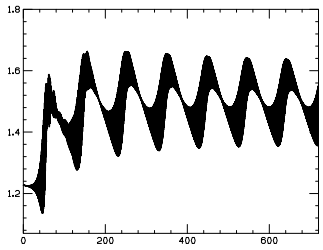

Figure 1: Bunch length σ_q vs. number of synchrotron periods, current vacuum chamber, $N = 2.99 \cdot 10^{10}$. The black band arises by fill-in from the rapid oscillations.

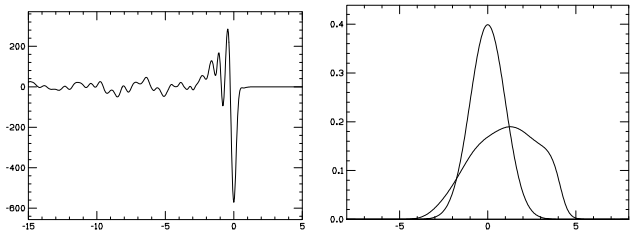

Figure 2: Wake potential $W(q)$ for previous chamber, and corresponding equilibrium charge distribution (unstable) for $N = 5 \cdot 10^{10}$, the latter compared to the Gaussian distribution for zero wake.

tion. In fact, the calculated sawtooth mode persists to much higher current, with the only fast frequency being near $2\omega_s$.

4 PREVIOUS VACUUM CHAMBER

In 1992-93 the vacuum chamber of each damping ring was replaced by a much smoother chamber. By eliminating strongly inductive impedance components, one hoped to raise the threshold current for bunch lengthening and achieve a smaller bunch length. It turned out that the threshold was in fact lowered, but SLC performance was nevertheless improved, because one could get a relatively short bunch and operate above threshold. It is clear that we are dealing with two very different types of instabilities for the old and new rings. The instability of the new ring is in some sense weaker, and is thought to be associated with radial mode coupling in an impedance which is now mainly resistive [2](1995). Since these matters are still not well understood, it is interesting to compare calculations for the old and new rings. Experimental results for the old ring are mostly unpublished, less systematic, and strongly dependent on r.f. voltage and beam current. We have yet to make detailed comparisons with the present method of simulation.

Here we give first results for one r.f. voltage, namely 800 KeV. The other relevant parameters are $\sigma_E = 0.805\mathrm{MeV}$, $\sigma_z = 0.495\mathrm{cm}$, $\nu_s = f_s/f_r = 0.0117$, $f_r = 8.47\mathrm{MHz}$, $\beta = 1/(\omega_s \tau_d) = 9.46 \cdot 10^{-4}$.

Fig. 2 shows the wake function, and the corresponding equilibrium charge distribution (unstable) at the highest current we consider, $N = 5 \cdot 10^{10}$. The potential well distortion is remarkably large at this current. In agreement with Ref.[2], we find that this wake potential induces a large dipole oscillation. In machine operation the dipole mode is suppressed by Robinson damping. To simulate this damping we follow [2], adding a term $-2\langle p \rangle / (\omega_s \tau_R)$ to the expression for $dp/d\theta$, where $\langle p \rangle = \int p f(q,p,\theta) dq dp$. We choose the damping time τ_R to be the synchrotron period, but find that considerably larger τ_R gives about the same result. This damping is important for stability of our algorithm for long times. It was not necessary in our previous calculations for the new chamber [3].

Figures 3 through 9 show the normalized r.m.s. energy spread, σ_p, versus the number of synchrotron periods, for increasing current. Of course, the graphs for σ_q are quite similar in appearance. The total time interval of 1380 synchrotron periods corresponds to more than 8 longitudinal damping times (168 periods per damping time), about twice the typical storage time. The apparent stability of the numerical integration for such a long time is noteworthy. Of course, stability is not the same thing as accuracy, and a fully convincing validation of these results has not yet been made.

At $N = 2 \cdot 10^{10}$ the equilibrium distribution is invariant to high accuracy. The threshold for bunch lengthening and increased energy spread is at about $2.25 \cdot 10^{10}$. The experimental threshold was approximately $3 \cdot 10^{10}$. As indicated in Fig. 4, we find a huge energy spread already at $2.5 \cdot 10^{10}$, but it comes and goes with a very long period, 3.7 damping times. The fast oscillations have frequency close to $2\omega_s$. As the current is increased this effect is more and more pronounced, until a transition to much different behavior occurs at $4 \cdot 10^{10}$; namely, a large initial spread evolving to an asymptotic sawtooth mode with lesser amplitude. The fast oscillations within the sawtooth have a frequency of about $3.3\omega_s$.

The period of the sawtooth envelope at $5 \cdot 10^{10}$ is about $1/4$ of a damping time, in good agreement with the macroparticle simulation of Ref. [2] at the same current. The latter was done with a damping time reduced by a factor of 10 from the correct value, however. We find that the qualitative behavior of high-current modes depends strongly on the damping rate. Figure 10 shows our result with a 10-fold reduction in damping time, over an interval of 3 reduced damping times. This disagrees strongly with the result of [2] on the same interval, which resembled more our Fig. 9. Although the disagreement is disappointing, it perhaps serves as a good reminder of the subtlety and complication of high-current coherent motion. Also, one should remember that the models of radiation are mathematically different in the macroparticle and VFP approaches, even if the underlying physical pictures are similar. In the VFP model the radiation is spread more uniformly around the ring.

To analyze the modal structure of the distribution, we make a Fourier analysis of the charge density $\rho(q,\theta)$ [3].

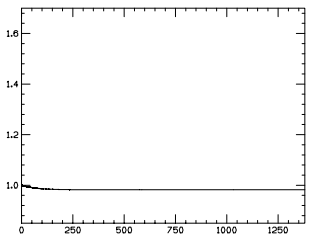

Figure 3: $N = 2 \cdot 10^{10}$

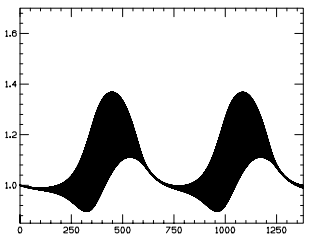

Figure 4: $N = 2.5 \cdot 10^{10}$

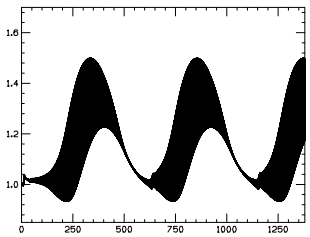

Figure 5: $N = 3 \cdot 10^{10}$

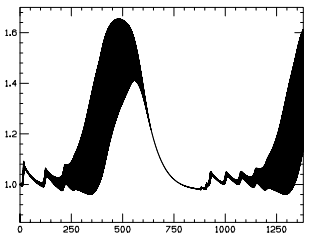

Figure 6: $N = 3.5 \cdot 10^{10}$

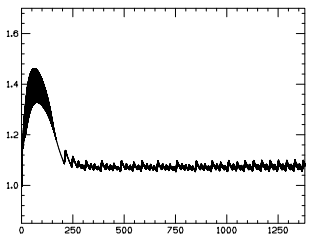

Figure 7: $N = 4 \cdot 10^{10}$

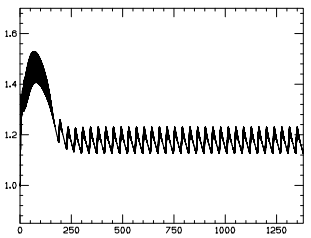

Figure 8: $N = 4.5 \cdot 10^{10}$

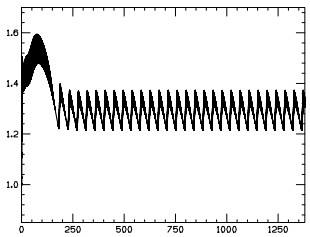

Figure 9: $N = 5 \cdot 10^{10}$

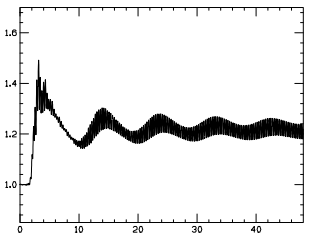

Figure 10: $N = 5 \cdot 10^{10}$, damping time reduced by factor of 10.

We first make a Fourier transform with respect to q, obtaining $\hat{\rho}(\omega, \theta)$, and fix ω at a typical revolution harmonic that can be seen in frequency analysis of a BPM signal, namely 10 GHz. Then we do a periodic Fourier analysis with respect to θ, on the long period of the sawtooth mode. The result for the power spectrum at $N = 5 \cdot 10^{10}$ is shown in Fig.11; the abscissa is frequency in units of ω_s. The strong line at the revolution harmonic is suppressed. The "sextupole" peak centered at $3.3\omega_s$ agrees well with [2] and with experimental experience in which a frequency near 3 was often seen. At other currents above the sawtooth threshold the result is pretty much the same, with little shift in frequency with current. On the other hand, below the sawtooth threshold we get a "quadrupole" peak like that for $N = 2.5 \cdot 10^{10}$ at $1.85\omega_s$, shown in Fig.11.

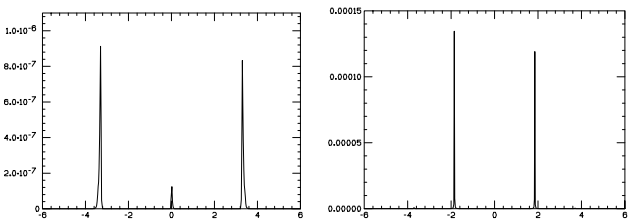

Figure 11: Sidebands of 10GHz revolution harmonic at $N = 5 \cdot 10^{10}$ (left) and $N = 2.5 \cdot 10^{10}$ (right)

Again, there is little dependence on current. The behavior *vs.* current is surprising in view of earlier simulations and experiments, and deserves further study.

5 REFERENCES

[1] K. Oide, *Proc. 4th Adv. ICFA Beam Dynamics Workshop, KEK, 1991*; KEK Preprint 94-138 (1994).

[2] K. Bane and K. Oide, *Proc. 1995 IEEE PAC, Dallas*; *Proc. 1993 IEEE PAC, Washington*.

[3] R. Warnock and J. Ellison, *Proc. 2nd ICFA Workshop on High Brightness Beams, UCLA, 1999*, preprint SLAC-PUB-8404 (2000).